processes

MDPI

Article

Experimental Study on Forced Convection Heat Transfer from Plate-Fin Heat Sinks with Partial Heating

Jae Jun Lee, Hyun Jung Kim and Dong-Kwon Kim *

Department of Mechanical Engineering, Ajou University, Suwon 16499, Korea; sweeperlee@ajou.ac.kr (J.J.L.); hyunkim@ajou.ac.kr (H.J.K.)

* Correspondence: dkim@ajou.ac.kr

Received: 4 September 2019; Accepted: 18 October 2019; Published: 21 October 2019

Abstract: In this study, plate-fin heat sinks with partial heating under forced convection were experimentally investigated. The base temperature profiles of the plate-fin heat sinks were measured for various heating lengths, heating positions, flow rates, and channel widths. From the experimental data, the effects of heating length, heating position, and flow rate on the base temperature profile and the thermal performance were investigated. Finally, the characteristics of the optimal heating position were investigated. As a result, it was shown that the optimal heating position was on the upstream side in the case of the heat sinks under laminar developing flow, as opposed to the heat sinks under turbulent flow. It was also shown that the optimal heating position could change significantly due to heat losses through the front and back of the heat sink, while the effects of the heat loss through the sides of the heat sink on the optimal heating position were negligible. In addition, it was shown that the one-dimensional numerical model with empirical coefficients could predict the important trends in the measured temperature profiles, thermal resistances, and optimal heating lengths.

Keywords: plate-fin heat sink; partial heating; forced convection

1. Introduction

The demand for high-performance and compact products has resulted in a continuous increase in heat dissipation from electronic devices in various systems, such as power converters, supercomputers, and electric vehicles [1,2]. The high heat dissipation from electronic products results in a high junction temperature, which negatively affects the overall performance and durability of the product. Therefore, efficient cooling of these devices is essential and various cooling methods have been developed. In addition, the efficient cooling is also essential for various thermal systems such as transcritical CO_2 refrigeration systems [3], ice storage tanks [4], wind tunnels [5], and heat exchanger/reactors [6]. The most common cooling method is the use of plate-fin heat sinks under forced convection. Therefore, many previous studies have focused on plate-fin heat sinks [7–11]. The thermal performance of these heat sinks is best when the heated base area is equal to the total base area, because the spreading resistance is minimized [12]. However, in many cases, the total base area of the heat sink is larger than the heated base area, as shown in Figure 1. It is because the amount of heat dissipation increases as the total base area increases, and the large total base area is required to sufficiently dissipate heat from high-performance and compact electronic devices, in many cases. For example, small Insulated Gate Bipolar Transistors (IGBTs) are generally mounted on large heat sinks in power electronics [13].

Many researchers have investigated the thermal performance of plate-fin heat sinks with partial heating under forced convection. These research works are well-summarized in Yoon et al. [14]. For example, Culham et al. investigated the role of spreading resistance of the heat sink base caused by partial heating in the design and the selection of the plate-fin heat sinks [15]. They showed that the spreading resistance could be significant without proper thermal design of the heat sinks. Ellison analytically solved a three-dimensional heat conduction equation for obtaining temperature fields in the heat sink bases and for calculating spreading resistances for various heat source sizes [16]. He showed that his results could be used for designing plate-fin heat sinks. Cho et al. experimentally investigated the effects of non-uniform mass flow distributions and heat flux conditions on the thermal performance of microchannel heat sinks [17]. They observed that the microchannel heat sink should be designed by considering the heat flux conditions. Yoon et al. also experimentally investigated the thermal performance of plate-fin and strip-fin minichannel heat sinks, under partial heating [18]. Lelea analyzed the effects of the heating position on the thermal performance of a microchannel heat sink by numerically solving the conjugate heat transfer problem [19]. He observed that the heating position influences the thermal characteristics and that upstream heating has a better thermal performance than central or downstream heating. Toh et al. also numerically calculated the three-dimensional velocity and temperature fields in a partially heated microchannel heat sink by using a finite volume method [20]. Although all of these studies are systematic and provide useful results, they used water or refrigerant as the working fluid and focused on minichannel heat sinks or microchannel heat sinks. As a result, the information which these studies provide for macroscale heat sinks with air as the working fluid is limited. However, macroscale heat sinks with air as the working fluid are commonly used in various systems. Therefore, there have been several studies for investigating the thermal performance of macroscale plate-fin heat sinks under partial heating with air as the working fluid. For example, Emekwuru et al. numerically investigated the influence of three different partial heating positions on the thermal performance of air-cooled macroscale heat sinks [21]. They showed that the thermal resistance is minimized when the partial heating position is centrally located, for most Reynolds numbers. Yoon et al. extensively conducted numerical studies on the thermal performance of plate-fin heat sinks according to the partial heating position to determine the optimal heating position [14]. They showed that the thermal performance is maximized when the heating position is located on the downstream side near the center of the heat sink.

However, first, to the best of our knowledge, intensive experimental studies on the thermal performances of macroscale plate-fin heat sinks under partial heating with air as the working fluid have not been systematically conducted for various heating locations, flow rates, and channel widths. In particular, previous studies on macroscale plate-fin heat sinks [14,21] was focused on heat sinks under turbulent flows with very high flow rates, and it is uncertain whether their conclusions are applicable for heat sinks under laminar developing flows with low flow rates.

Second, heat sinks used in the practical situation showed heat losses through the front, back, and sides of the heat sink ($q_{loss,f}$, $q_{loss,b}$, and $q_{loss,s}$ in Figure 1). However, there were no previous studies on the effects of these heat losses on the optimal heating position of macroscale plate-fin heat sinks under partial heating.

Third, a full three-dimensional numerical simulation could estimate the thermal performance accurately but required a time-consuming code writing process. In addition, commercial numerical simulation programs might have cost issues. Therefore, sometimes it is useful to perform several experiments and to investigate the effects of important engineering parameters on thermal performance by using a one-dimensional model that can predict experimental results.

In this study, plate-fin heat sinks under partial heating with air as the working fluid were experimentally investigated. The base temperature profiles of plate-fin heat sinks under laminar developing flows were measured for various heating lengths, heating positions, flow rates, and channel widths. From the experimental data, the effects of various engineering parameters on the base temperature profile and the thermal performance were investigated. Finally, the characteristics of the optimal heating position were investigated. It is shown that the conclusions of the previous studies [14,21] on optimal heating position of plate-fin heat sink under turbulent flow did not apply

to the heat sink under the laminar developing flow examined in this study. In is also shown that the optimal heating position could change significantly due to heat losses through the front and back of the heat sink. In addition, a simple one-dimensional numerical model for predicting the thermal performances is presented.

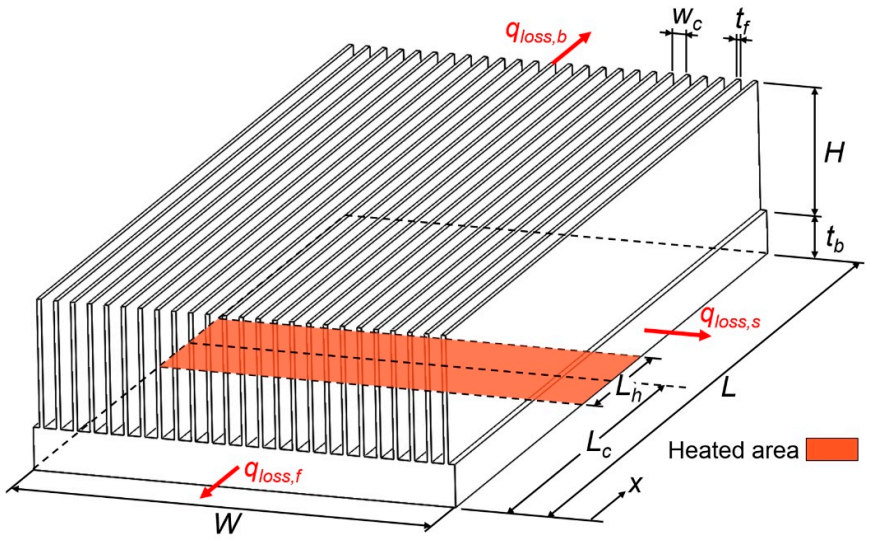

Figure 1. Plate-fin heat sinks with partial heating.

2. Experimental Procedure

A schematic diagram of a heat sink is shown in Figure 1. The length *L*, width *W*, height *H*, base thickness t_b, and fin thickness t_f of the heat sink were 20 cm, 10 cm, 3 cm, 1 cm, and 1 mm, respectively. The experiment was conducted for five different combinations of heating lengths and heating positions, four different flow rates, and two different channel widths, as listed in Table 1. In this table, *N*, w_c, L_h, and L_c are the fin number, channel width, heated length, and the distance from the upstream end to the center of the heated area, respectively. The heat sink was made of SUS304 (k = 16.2 W/m K). As shown in Figure 2, 22 T-type thermocouples were attached to the base of the heat sink. More specifically, in order to measure the profile of the base temperature T_b along the flow direction, thermocouples were installed at 11 points in the x direction. The thermocouples were attached at two points in the y direction to check that the measured base temperature profile along the flow direction was reliable. Silver epoxy was used to minimize contact thermal resistance between the thermocouple and the base. Four other T-type thermocouples were placed at the inlet of the test section to measure the ambient temperature T_{amb}. As shown in Figure 3, the signals from the thermocouples were converted to temperature data using a data acquisition system (34970A DAQ; Agilent Technology) and were stored in a computer. As shown in Figure 2, five film heaters of the same size were attached to the bottom surface of the heat sink base to locally apply heat to the heat sink. The film heater was made of SUS304 and was attached using a Kapton tape. These five heaters were powered and controlled by a DC power supply (PL-3005D; Protek) to be turned on and off, independently.

The total power input to the heater was fixed at 40 W. Five different combinations of heating lengths and heating positions were investigated in this study, as listed in Table 1. As shown in Figure 3, the heat sink with the attached thermocouples and heaters was installed inside a rectangular duct in acrylic. The duct was connected to a wind tunnel system with a nozzle flow meter and a blower (TB-150; Innotech) to measure the flow rate of air while generating air flow in the duct. The nozzle flow meter consisted of the nozzle and the differential pressure meter (FCO332; Furness Controls), and it measured the volume flow rate by measuring pressure difference between the inlet and the outlet of the nozzle caused by flow restriction by the nozzle. Four different flow rates were investigated in this study, as listed in Table 1. Each measurement was repeated three times to ensure the reliability of data. The temperature was measured until the temperature change dropped to less

than 0.1 °C for 10 min. After the experiment, the uncertainty of the data were analyzed, and details of the analysis were described in Reference [22] and Appendix A.

Table 1. Design parameters for the experiment.

N	w_c [mm]	L_h/L	L_c/L	Flow rate Q [m³/min]
25	3	1.0	0.5	0.2, 0.4, 0.6, 0.8
		0.6	0.5	0.2, 0.4, 0.6, 0.8
		0.2	0.3	0.2, 0.4, 0.6, 0.8
			0.5	0.2, 0.4, 0.6, 0.8
			0.7	0.2, 0.4, 0.6, 0.8
13	7	1.0	0.5	0.2, 0.4, 0.6, 0.8
		0.6	0.5	0.2, 0.4, 0.6, 0.8
		0.2	0.3	0.2, 0.4, 0.6, 0.8
			0.5	0.2, 0.4, 0.6, 0.8
			0.7	0.2, 0.4, 0.6, 0.8

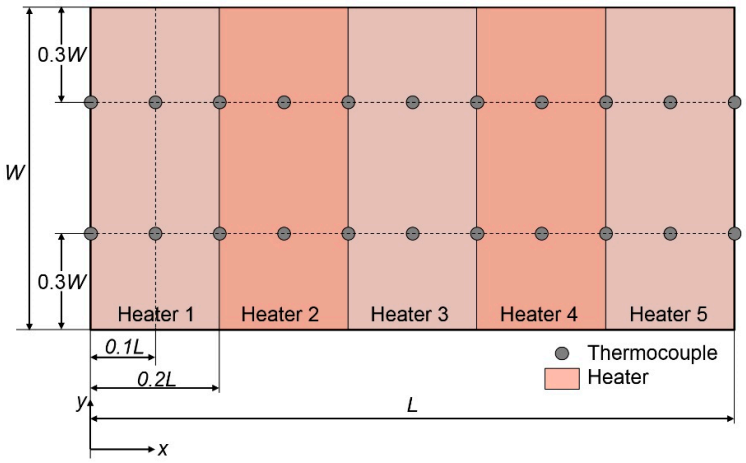

Figure 2. Positions of thermocouples and heaters on the heat sink base.

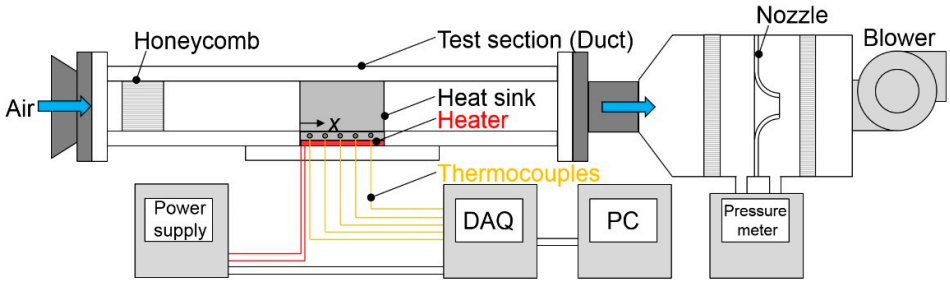

Figure 3. Schematic diagram of the experimental setup.

3. Results

Figure 4a–e show the profiles of the difference between the base temperature T_b and the ambient temperature T_{amb}, along the flow direction for five different combinations of heating lengths and heating positions and four different flow rates when the channel width was 7 mm. The various trends of the temperature profile observed in these figures were as follows.

(a) In all cases shown in Figure 4a–e, regardless of the value of x, the base temperature decreased as the flow rate increased. This was mainly because the temperature of the fluid flowing inside the heat sink decreased as the flow rate increased. This was also because the local heat transfer

coefficient, which was inversely proportional to the temperature difference between the fluid temperature and the base temperature, increased as the flow rate increased.

(b) The extent to which the base temperature decreased with an increase in the flow rate, decreased as the flow rate increased.

(c) The point at which the base temperature was maximized always existed in the portion where the heat sink was heated. When the size of the heating portion was equal to the size of the heat sink, the point at which the base temperature was maximized lay almost at the end of the heating portion where x was the largest. When the size of the heating portion was much smaller than the size of the heat sink, the point where the base temperature was maximized was almost at the center of the heating portion.

(d) The base temperature at $x = L_c + \Delta x$ was larger than the base temperature at $x = L_c - \Delta x$, regardless of the value of Δx. This was mainly because the fluid temperature monotonically increased as x increased.

(e) As shown in Figure 4a, when the heat sink was uniformly heated, the base temperature increased monotonically with an increase in x. This was because the temperature of the fluid increased as x increased. This was also because the heat transfer coefficient, which was inversely proportional to the temperature difference between the fluid temperature and the base temperature, decreased as x increased.

Figure 5a–e show the profiles of the difference between the base temperature T_b and the ambient temperature T_{amb} along the flow direction when the channel width was 3 mm. The trends in the temperature profile were consistent with the previously described trends for the channel width of 7 mm.

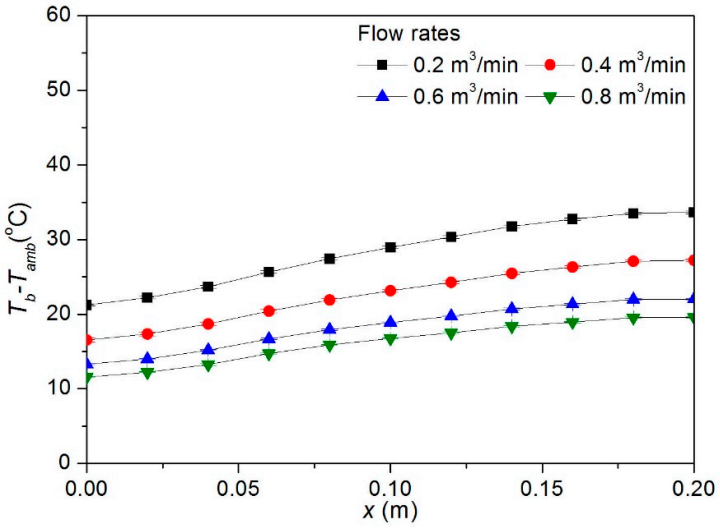

(**a**)

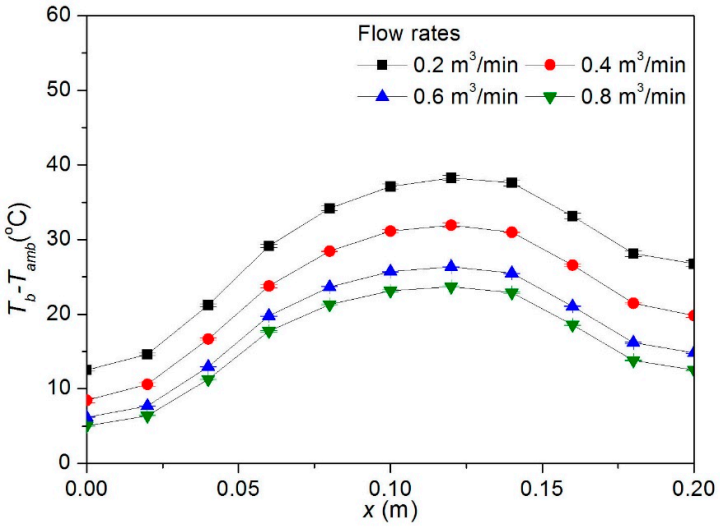
Flow rates
0.2 m³/min
0.4 m³/min
0.6 m³/min
0.8 m³/min
T_b-T_{amb}(°C)
x (m)
0
10
20
30
40
50
60
0.00
0.05
0.10
0.15
0.20

(**b**)

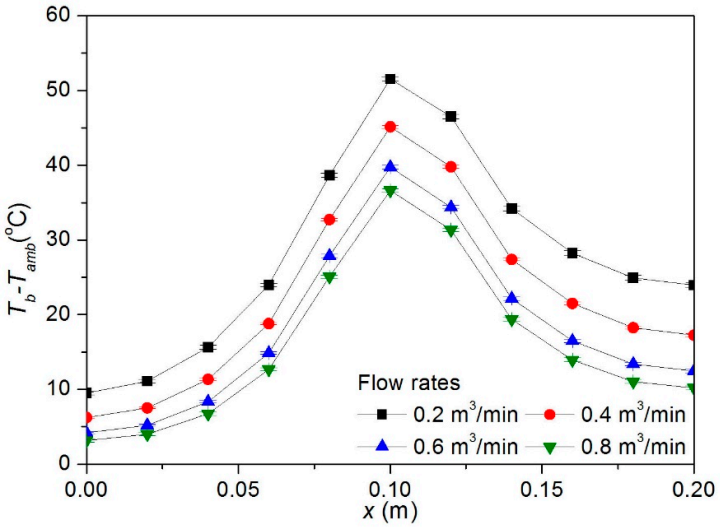
Flow rates
0.2 m³/min
0.4 m³/min
0.6 m³/min
0.8 m³/min
T_b-T_{amb}(°C)
x (m)
0
10
20
30
40
50
60
0.00
0.05
0.10
0.15
0.20

(**c**)

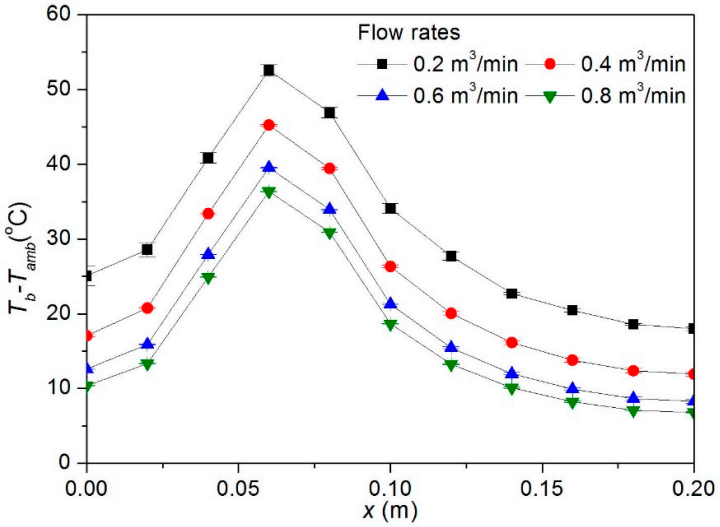
Flow rates
0.2 m³/min
0.4 m³/min
0.6 m³/min
0.8 m³/min
T_b-T_{amb}(°C)
x (m)
0
10
20
30
40
50
60
0.00
0.05
0.10
0.15
0.20

(**d**)

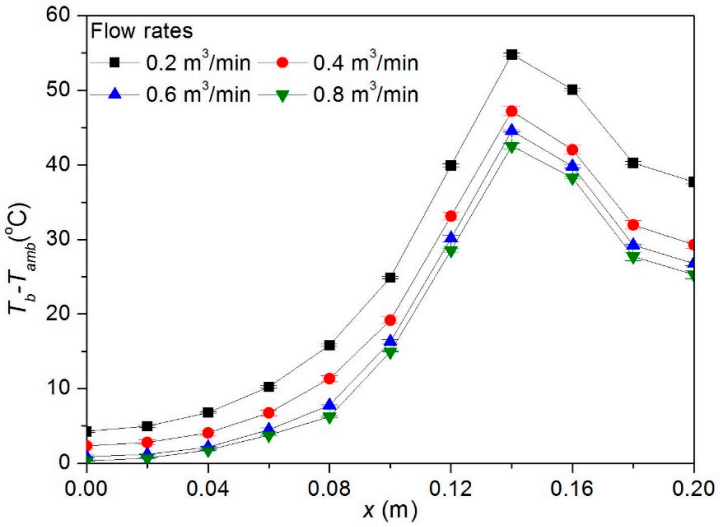

(**e**)

Figure 4. Profiles of difference between base temperature and ambient temperature (w_c = 7 mm). (**a**) L_h/L = 1.0, L_c/L = 0.5; (**b**) L_h/L = 0.6, L_c/L = 0.5; (**c**) L_h/L = 0.2, L_c/L = 0.5; (**d**) L_h/L = 0.2, L_c/L = 0.3; and (**e**) L_h/L = 0.2, L_c/L = 0.7.

Figure 6a,b show the thermal resistances for five different combinations of heating lengths and heating positions, four different flow rates, and two different channel widths. Here, the thermal resistance R was defined as the difference between the maximum temperature of the heat sink base $T_{b,max}$ and the ambient temperature T_{amb} divided by the amount of heat q applied to the heat sink. Therefore,

$$R = \frac{T_{b,max} - T_{amb}}{q}. \quad (1)$$

The various characteristics of thermal resistance observed in these figures are as follows.

(a) Regardless of the heating position and channel width, the thermal resistance decreased monotonically as the flow rate increased. This was because the temperature of the cooling fluid filling the inside of the heat sink decreased as the flow rate increased.

(b) Regardless of the channel width and flow rate, the thermal resistance increased as the heating length decreased. This was because the heat sink base was more heavily heated locally, owing to an increase in heat flux (amount of heat per unit area) applied to the heated portion of the heat sink base as the heating length decreased. When the heat sink base was uniformly heated, heat was uniformly dissipated from the heat sink to the fluid through the heat sink surface. In contrast, only a part of the surface was mainly used for the heat dissipation in the case of the locally heated heat sink.

(c) There was an optimal heating position that minimized the thermal resistance when the heating length was fixed. However, as shown in Figure 6a, the optimal heating position was not fixed and could be changed by changing the flow rate.

Finally, to investigate the characteristics of characteristics of the optimal heating position, we developed a relatively simple one-dimensional numerical model that could roughly predict the experimental results (further explanation on a one-dimensional numerical model is given in Appendix B). Finally, Figure 7 shows the thermal resistances for various heating positions and flow rates when the heating length was fixed. The characteristics of the optimal heating position observed from Figure 7 were as follows.

(a) When the flow rate was fixed, there was an optimal heating position that minimized the thermal resistance.

(b) The optimal heating position was not independent of the flow rate. In this study, the optimal heating position moved toward the smaller x as the flow rate increased. Therefore, when controlling the flow rate from the fan in an actual situation, this fact should be considered to determine the heating position.

(c) If the heating position moved slightly in the positive x direction or in the negative x direction from the optimal heating position, the thermal resistance did not increase significantly. Therefore, in an actual situation, a slight change of the heating position from the optimal heating position was acceptable.

(d) However, if the heating position was far from the optimal heating position, the thermal resistance could be very large. Therefore, in an actual situation, the heating position should not be close to the front or rear ends of the heat sink.

(e) As presented earlier, Emekwuru et al. showed that the thermal resistance was minimized when the heating position was centrally located for most Reynolds numbers [21]. On the other hand, Yoon et al. showed that the thermal performance was maximized when the heating position was located on the downstream side near the center of the heat sink [14]. However, these conclusions from the previous studies did not apply to the situation examined in this study. Figure 7 indicates that the thermal performance was maximized when the heating position was located on the upstream side. In addition, Figure 6a also shows that the optimal heating position was located on the upstream side in some cases. The main reason why the conclusions from the previous studies did not apply to the situation examined in this study was that the previous study was focused on heat sinks under turbulent flows with very high flow rates and the present experiments were conducted for heat sinks under laminar developing flows. The fact that Lelea also observed that upstream heating had a better thermal performance than central or downstream heating for the heat sink under laminar flow in his study [19] supported this reasoning, although his study was focused on water-cooled microchannel heat sinks.

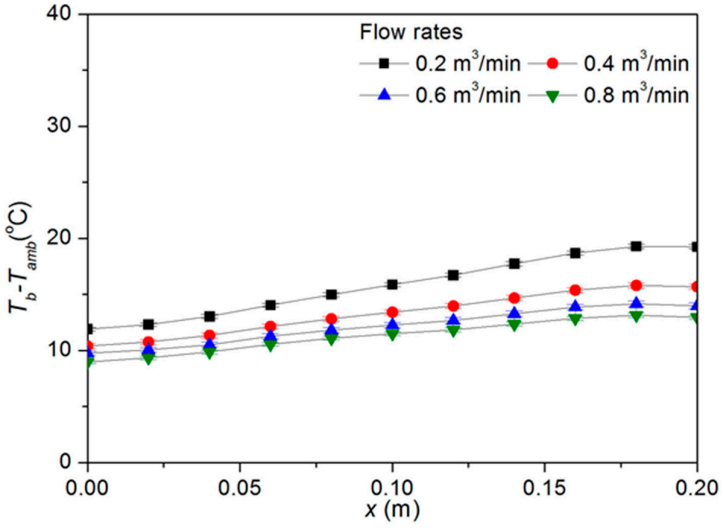

(**a**)

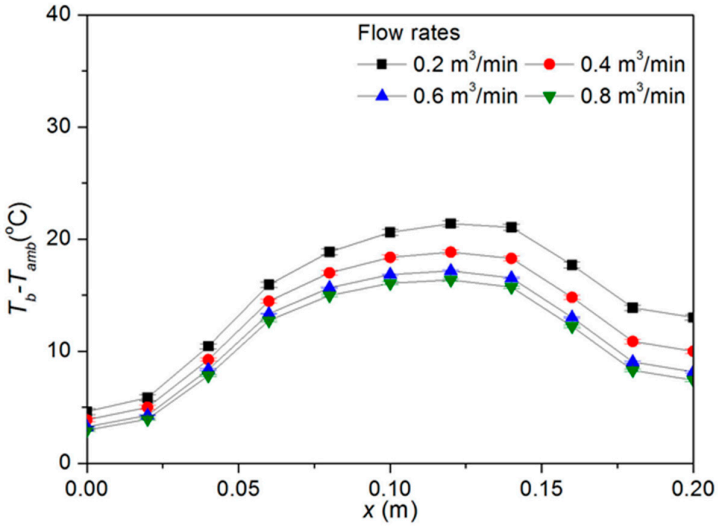
Flow rates
0.2 m³/min
0.4 m³/min
0.6 m³/min
0.8 m³/min
T_b-T_{amb}(°C)
x (m)
0
10
20
30
40
0.00
0.05
0.10
0.15
0.20

(**b**)

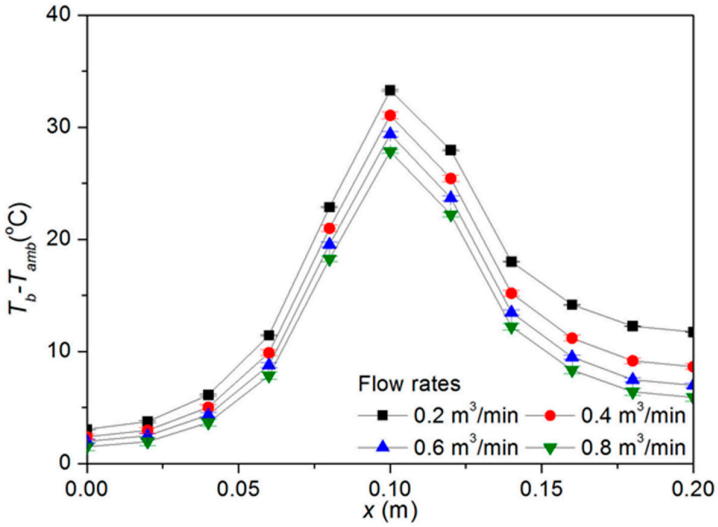
Flow rates
0.2 m³/min
0.4 m³/min
0.6 m³/min
0.8 m³/min
T_b-T_{amb}(°C)
x (m)
0
10
20
30
40
0.00
0.05
0.10
0.15
0.20

(**c**)

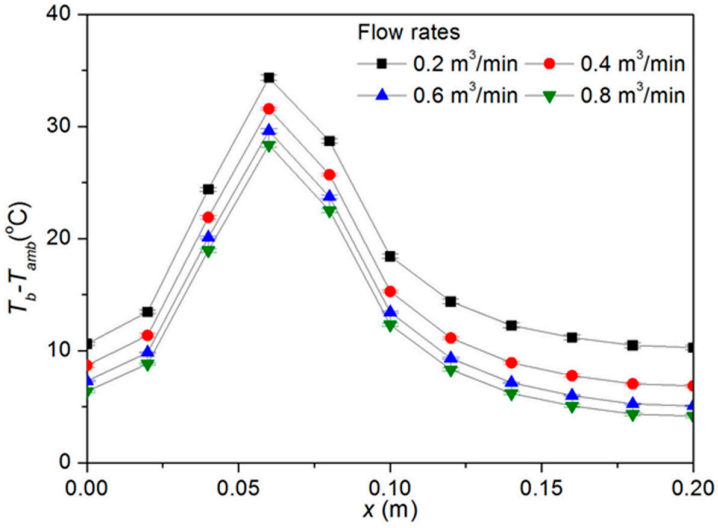
Flow rates
0.2 m³/min
0.4 m³/min
0.6 m³/min
0.8 m³/min
T_b-T_{amb}(°C)
x (m)
0
10
20
30
40
0.00
0.05
0.10
0.15
0.20

(**d**)

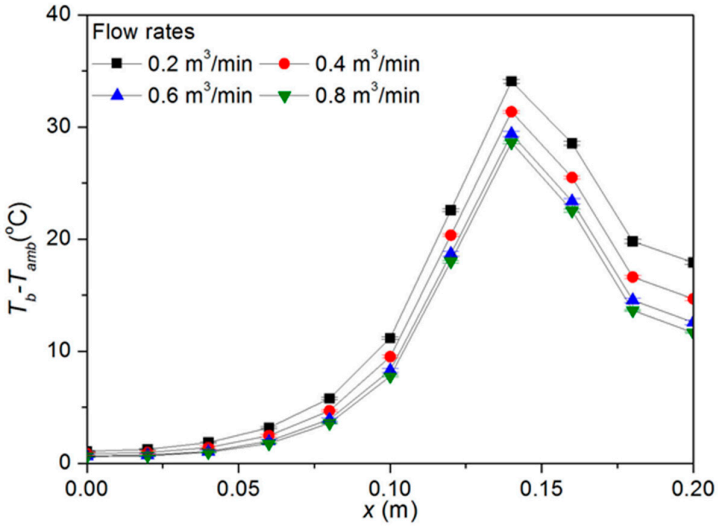

(**e**)

Figure 5. Profiles of difference between base temperature and ambient temperature (w_c = 3 mm). (**a**) L_h/L = 1.0, L_c/L = 0.5; (**b**) L_h/L = 0.6, L_c/L = 0.5; (**c**) L_h/L = 0.2, L_c/L = 0.5; (**d**) L_h/L = 0.2, L_c/L = 0.3; and (**e**) L_h/L = 0.2, L_c/L = 0.7.

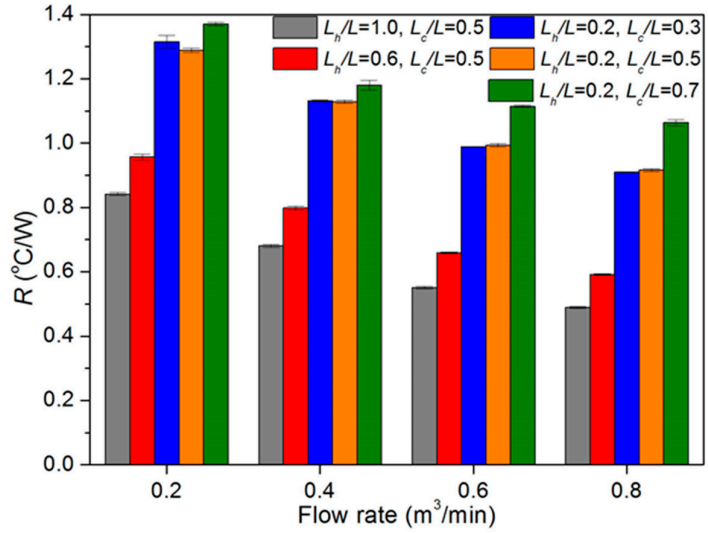

(**a**)

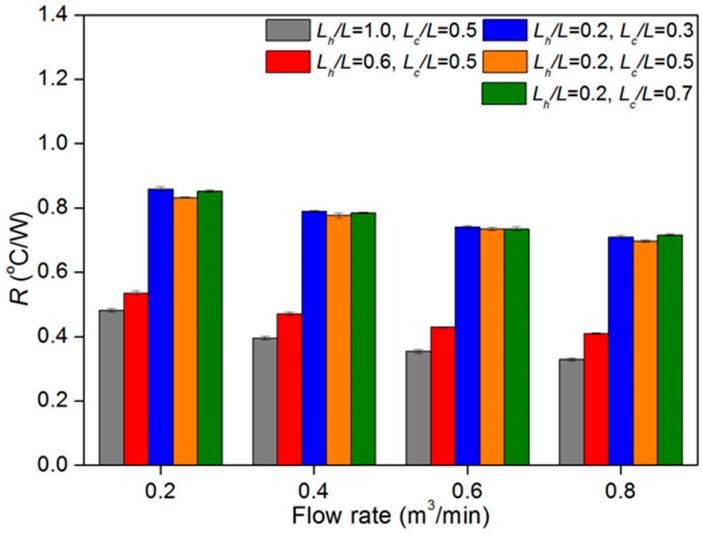

Figure 6. Thermal resistances. (**a**) w_c = 7 mm; and (**b**) w_c = 3 mm.

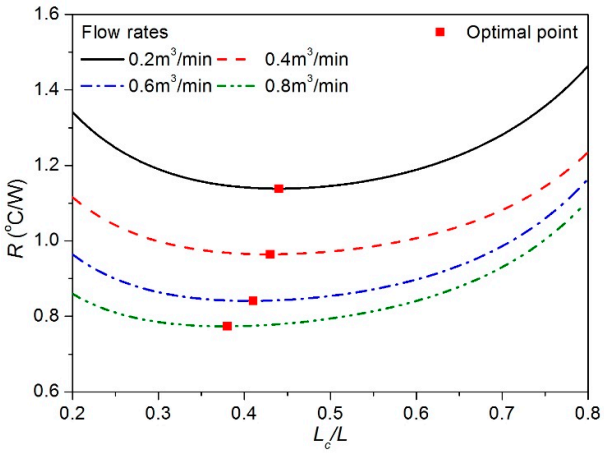

Figure 7. Thermal resistances for various heating positions and flow rates (w_c = 7 mm, L_h/L = 0.2).

The heat sinks used in the practical situations showed heat losses through the front, back, and sides of the heat sink ($q_{loss,f}$, $q_{loss,b}$, and $q_{loss,s}$ in Figure 1). Therefore, in this study, effects of these heat losses on the optimal heating position were investigated. Figures 8–10 show the thermal resistances of the heat sinks calculated by one-dimensional models for various thermal resistances for the heat losses through the front, back, and sides of the heat sinks, respectively. In these figures, $R_{loss,f}$ and $R_{loss,b}$ are the thermal-resistances-related heat losses through the front and back of the heat sink, respectively. $R'_{loss,s}$ is the thermal resistance per unit length related to heat loss through the sides of the heat sink, as explained in Appendix B. The characteristics of the optimal heating position observed in Figures 8–10 were as follows.

(a) The optimal heating position could change significantly due to heat losses through the front and back of heat sink. Therefore, even when the heat sink with the same dimensions was under the same flow rate, the optimal heating position could be completely different depending on how the heat sink was connected to the other devices in the thermal system.
(b) The optimal heating position moved toward the smaller x as the heat loss through the front of the heat sink increased.
(c) The optimal heating position moved toward the larger x as the heat loss through the back of the heat sink increased.

(d) The optimal heating position was almost independent to the heat loss through the sides of the heat sink.

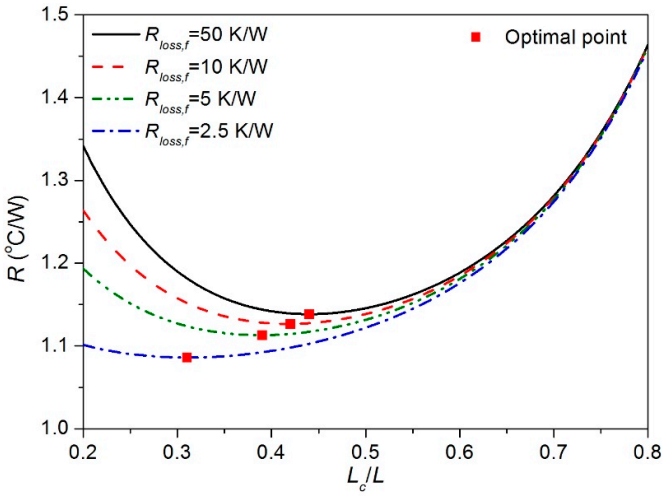

Figure 8. Thermal resistances for various heat losses through the front of the heat sink (Q = 0.2 m³/min, w_c = 7 mm, L_h/L = 0.2).

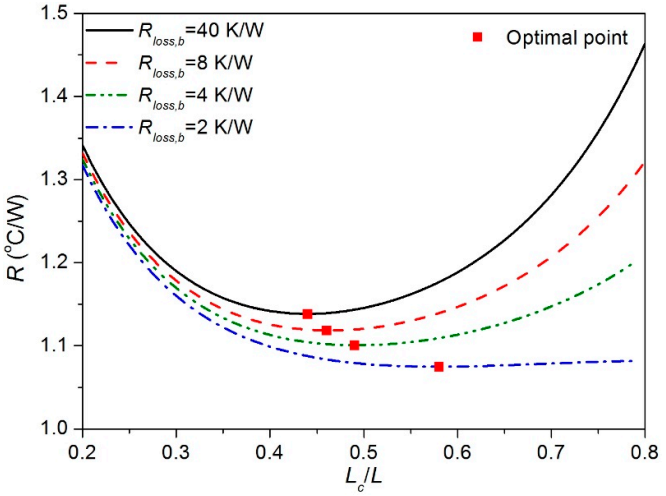

Figure 9. Thermal resistances for various heat losses through the back of the heat sink (Q = 0.2 m³/min, w_c = 7 mm, L_h/L = 0.2).

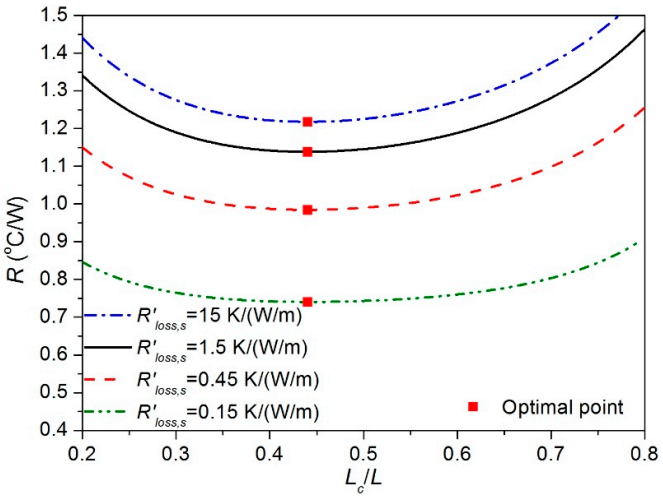

Figure 10. Thermal resistances for various heat losses through the sides of the heat sink (Q = 0.2 m^3/min, w_c = 7 mm, L_h/L = 0.2).

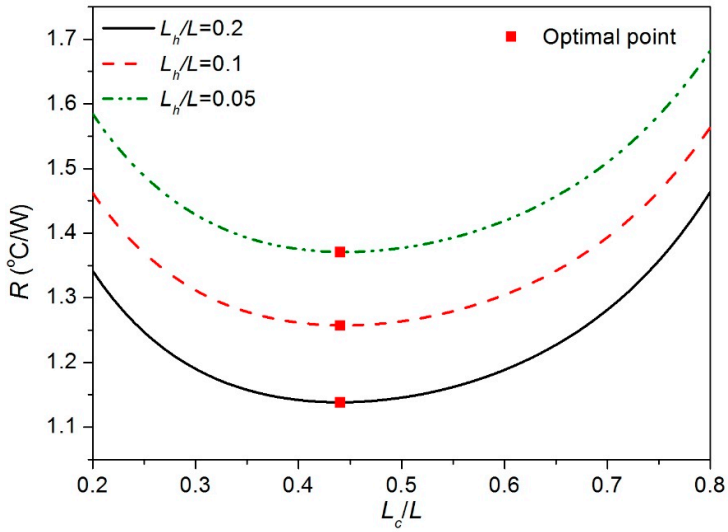

Figure 11. Thermal resistances for various heated lengths (Q = 0.2 m^3/min, w_c = 7 mm).

In addition, Figure 11 shows the thermal resistances for various heated lengths. As shown in the figure, the optimal heating position also did not depend strongly on the heated length, if the change in heat transfer coefficient due to the heated length was not significant.

4. Conclusions

In this study, macroscale plate-fin heat sinks under partial heating with air as the working fluid were experimentally investigated. The base temperature profiles of the plate-fin heat sinks under laminar developing flows were measured for various heating lengths, heating positions, flow rates, and channel widths. From the experimental data, the effects of various engineering parameters on the base temperature profile and the thermal performance were investigated. Finally, the characteristics of the optimal heating position were investigated.

The following were the new findings on the optimal heating position of the partially heated plate-fin heat sinks:

(a) The optimal heating position was on the upstream side in the case of the heat sinks under a laminar developing flow that were investigated in the present study. On the contrary, as shown

in a previous study [14], the optimal heating position was on the downstream side in the case of the heat sinks under turbulent flow.

(b) The optimal heating position could change significantly due to heat losses through the front and back of heat sink. Therefore, even when the heat sink with the same dimensions was under the same flow rate, the optimal heating position could be completely different depending on how the heat sink was connected to other devices in the thermal system.

(c) The optimal heating position was independent to the heat loss through the sides of the heat sink. The optimal heating position also did not depend strongly on the heated length.

(d) The one-dimensional numerical model with empirical coefficients could reflect the important trends in the measured temperature profiles, thermal resistances, and optimal heating lengths.

In addition, the following are some characteristics of the partially heated plate-fin heat sinks presented in this study:

(a) The point at which the base temperature was maximized always existed in the portion where the heat sink was heated. When the size of the heating portion was equal to the size of the heat sink, the point at which the base temperature was maximized lay almost at the end of the heating portion where x was the largest. When the size of the heating portion was much smaller than the size of the heat sink, the point where the base temperature was maximized was almost at the center of the heating portion.

(b) Regardless of the heating position and the channel width, the thermal resistance decreased monotonically as the flow rate increased. Regardless of the channel width and flow rate, the thermal resistance increased as the heating length decreased.

(c) The optimal heating position was not independent of the flow rate.

(d) If the heating position moved slightly in the positive x direction or in the negative x direction from the optimal heating position, the thermal resistance did not increase significantly. However, if the heating position was far from the optimal heating position, the thermal resistance could be very large.

Author Contributions: J.J.L. and D.-K.K. conducted the investigation; D.-K.K. and H.J.K. performed the formal analyses; D.-K.K. wrote the manuscript.

Funding: This research was supported by Nano-Material Technology Development Program through the National Research Foundation of Korea (NRF) funded by Ministry of Science and ICT (NRF-2011-0030285).

Conflicts of Interest: The authors declare no conflict of interest. The funders had no role in the design of the study; in the collection, analyses, or interpretation of data; in the writing of the manuscript, or in the decision to publish the results.

Nomenclature

A_s	solid cross-sectional area
C_1, C_2, C_3, C_4	empirical coefficients
c_f	fluid heat capacity
H	height of heat sink
h	heat transfer coefficient
k_s	solid thermal conductivity
L	length of heat sink
L_c	distance from the upstream end to the center of the heated area
L_h	heated length
$\dot{m}$	mass flow rate
N	fin number
P	wetted perimeter
Q	flow rate
q	amount of heat applied to heat sink
Q'	heat input per unit length
$q_{loss,b}$	heat loss through the back of the heat sink
$q_{loss,f}$	heat loss through the front of the heat sink

$q_{loss,s}$	heat loss through the sides of the heat sink
R	thermal resistance
$R_{loss,b}$	thermal resistance related heat loss through the back of the heat sink
$R_{loss,f}$	thermal resistance related heat loss through the front of the heat sink
$R'_{loss,s}$	thermal resistance per unit length related to heat loss through the sides of the heat sink
T_{amb}	ambient temperature
T_b	base temperature
$T_{b,max}$	maximum temperature of the heat sink base
t_b	base thickness
t_f	fin thickness
W	width of heat sink
w_c	channel width
η_o	overall surface efficiency

Appendix A

Experimental Uncertainties

According to the manufacturers' calibration results, the instrument bias errors in the measurement are as shown in Table A1.

Table A1. Instrument bias errors.

Measurement Type	Error
Temperature	<0.5 K
Voltage	<0.01%
Current	<0.1%
Pressure	<0.5%

Appendix B

Detailed Explanation for the One-Dimensional Numerical Model

This appendix describes how to fit the thermal resistance as a function of flow rate and heating position by using a one-dimensional numerical model in this study.

The easiest method is to directly fit the thermal resistance shown in Figure 6 as a function of the heating position and flow rate by using some suitable functional form. However, if this method is used, the important trends in the measured temperature profiles shown in Figures 4 and 5 are ignored and not reflected, so there is a high probability that the results would not be engineeringly meaningful and would be less reliable.

Therefore, in this study, we developed a relatively simple one-dimensional numerical model with empirical coefficients that could roughly predict the temperature profiles. Then empirical coefficients were obtained by determining the values that minimized the root mean square error (RMSE) between the temperatures obtained through the experiment and the temperatures obtained from the numerical model. Finally, the thermal resistance was calculated as a function of the heating position and the flow rate from the model; presented in Figure 7.

Further explanation on the model is given as follows. According to References [23] and [24], the fluid temperature T_f and the base temperature T_b averaged in the direction perpendicular to the flow are given by the following Equations (A1) and (A2), respectively.

$$k_s A_s \frac{d^2 T_b}{dx^2} + \eta_o hP(T_f - T_b) - \frac{1}{R'_{loss,s}}(T_b - T_{amb}) + q' = 0 \quad \text{(A1)}$$

$$-\dot{m} c_f \frac{dT_f}{dx} + \eta_o hP(T_b - T_f) = 0 \quad \text{(A2)}$$

Here, k_s, A_s, η_o, h, P, $R'_{loss,s}$, q', $\dot{m}$, and c_f are the solid thermal conductivity, solid cross-sectional area, overall surface efficiency [25], heat transfer coefficient, wetted perimeter, thermal resistance per unit length related to heat loss through the sides of the heat sink ($q_{loss,s}$ in Figure 1), heat input per unit length, mass flow rate, and fluid heat capacity, respectively. The first and second terms in Equation (A1) are related to the conduction in the heat sink in the flow direction and the convection from the heat sink to the fluid, respectively. The third term is related to the heat loss from the heat sink to the surroundings in the direction perpendicular to the flow, and the fourth term is related to the heat input from the heater to the heat sink. The first and second terms in Equation (A2) are related to the fluid enthalpy change in the flow direction and the convection from the heat sink to the fluid, respectively. The governing equations were discretized by the control-volume-based finite difference method, and discretization equations were calculated using the Gauss–Seidel method.

The boundary conditions for these equations are given as follows.

$$T_f(x=0) = T_{amb} \tag{A3}$$

$$k_s A_s \left.\frac{dT_b}{dx}\right|_{x=0} = \frac{1}{R_{loss,f}}(T_b(x=0) - T_{amb}), k_s A_s \left.\frac{dT_b}{dx}\right|_{x=L} = -\frac{1}{R_{loss,b}}(T_b(x=L) - T_{amb}) \tag{A4}$$

The first boundary condition (Equation (A3)) indicated that the fluid temperature was at the ambient temperature at the inlet. The second boundary condition (Equation (A4)) indicated that there were heat losses in the -x direction from the upstream end face and in the +x direction from the downstream end face of the heat sink. In Equation (A4), $R_{loss,f}$ and $R_{loss,b}$ are the thermal resistances related heat losses through the front and back of the heat sink ($q_{loss,f}$ and $q_{loss,b}$, in Figure 1), respectively. To obtain the temperature profiles from the numerical model, we must know the value of the local heat transfer coefficient h. However, the exact value of the local heat transfer coefficient could be obtained only from a three-dimensional numerical analysis or from a precise bulk-mean fluid temperature measurement. However, such a complex numerical analyses or experiment was beyond the scope of this study, because the reason for using the numerical model in this study was to predict the tendency of the profile of temperatures qualitatively, using a simple method. Therefore, in this study, the local heat transfer coefficient was assumed to be as follows.

$$h = C_1(1 + C_2 L_c / L) - C_3(x/L)(1 + C_4 L_c / L) \tag{A5}$$

This equation is not perfect, but it reflects the following important facts. (a) As x increases, the local heat transfer coefficient tends to decrease. (b) The local heat transfer coefficient changes owing to the change in the heating position.

In this study, empirical coefficients were obtained by determining the values that minimized the root mean square error (RMSE) between the temperatures obtained through the experiment and the temperatures obtained from the numerical model.

$$RMSE = \sum_{i=1}^{11} \sqrt{T_{b,measured}(x_i) - T_{b,calculated}(x_i)} \tag{A6}$$

In Equation (A6), $T_{b,measured}$, $T_{b,calculated}$, and x_i are the measured base temperature, base temperature calculated from the model, and x coordinates of the measurements points, respectively. More specifically, the values of $R_{loss,f}$, $R_{loss,b}$, and $R_{loss,s}'$, which are not directly related to convective heat transfer, are obtained first by determining the values that minimize the RMSE for a uniformly heated heat sink without fluid flow, as shown in Figure A1. Subsequently, the remaining terms C_1, C_2, C_3, and C_4, which are related to convective heat transfer, are obtained by determining the values that minimize the RMSE for a partially heated heat sink with fluid flow, as shown in Figure A2 for example.

Figure A2 compares the profiles of the temperature difference between the base temperature and the ambient temperature calculated using the numerical model with the experimental results for several cases with the same heating length and different heating positions. It could be observed that

the base temperature profiles were qualitatively well-predicted by the model, although the simple numerical model could not perfectly predict the temperatures for all positions.

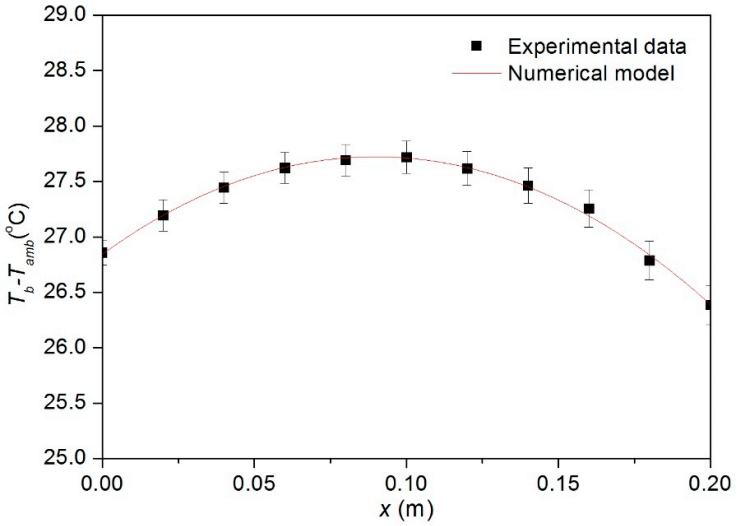

Figure A1. Comparison of temperature differences from experimental data and results of the numerical model for L_h/L of 1, channel width of 3 mm, flow rate of 0 m³/min, and heat input of 5 W.

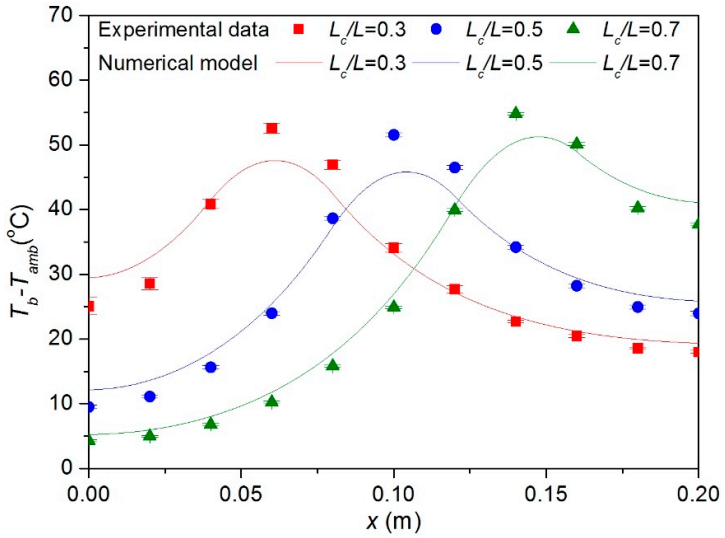

Figure A2. Comparison of temperature differences from experimental data and results of the numerical model for L_h/L of 0.2, channel width of 7 mm, and flow rate of 0.2 m³/min.

References

1. Mudawar, I. Assessment of high-heat-flux thermal management schemes. *IEEE Trans. Compon. Packag. Technol.* **2001**, *24*, 22–141.
2. Anandan, S.S.; Ramalingam, V. Thermal management of electronics: A review of literature. *Therm. Sci.* **2008**, *12*, 5–26.
3. Yang, J.; Ning, S. Experimental and Numerical Study of Double-Pipe Evaporators Designed for CO_2 Transcritical Systems. *Processes* **2019**, *7*, 547.
4. Zhou, H.; Chen, M.; Han, X.; Cao, P.; Yao, F.; Wu, L. Enhancement Study of Ice Storage Performance in Circular Tank with Finned Tube. *Processes* **2019**, *7*, 266.
5. Xue, R.; Ruan, Y.; Liu, X.; Chen, L.; Liu, L.; Hou, Y. Numerical Study of the Effects of Injection Fluctuations on Liquid Nitrogen Spray Cooling. *Processes* **2019**, *7*, 564.

6. He, M.; Li, Z.; Han, X.; Cabassud, M.; Dahhou, B. Development of a Numerical Model for a Compact Intensified Heat-Exchanger/Reactor. *Processes* **2019**, *7*, 454.
7. Teertstra, P.; Yovanovich, M.M.; Culham, J.R. Analytical forced convection modeling of plate fin heat sinks. *J. Electron. Manuf.* **2000**, *10*, 253–261.
8. Culham, J.R.; Muzychka, Y.S. Optimization of plate fin heat sinks using entropy generation minimization. *IEEE Trans. Compon. Packag. Technol.* **2001**, *24*, 159–165.
9. Jonsson, H.; Moshfegh, B. Modeling of the thermal and hydraulic performance of plate fin, strip fin, and pin fin heat sinks-Influence of flow bypass. *IEEE Trans. Compon. Packag. Technol.* **2001**, *24*, 142–149.
10. Iyengar, M.; Bar-Cohen, A. Least-energy optimization of forced convection plate-fin heat sinks. *IEEE Trans. Compon. Packag. Technol.* **2003**, *26*, 62–70.
11. Kim, D.K.; Jung, J.; Kim, S.J. Thermal optimization of plate-fin heat sinks with variable fin thickness. *Int. J. Heat Mass Transf.* **2010**, *53*, 5988–5995.
12. Muzychka, Y.S.; Yovanovich, M.M.; Culham, J.R. Influence of geometry and edge cooling on thermal spreading resistance. *J. Thermophys Heat Transfer*, **2006**, *20*, 247–255.
13. Musallam, M.; Johnson, C.M. Real-time compact thermal models for health management of power electronics. *IEEE Trans. Power Electron.* **2010**, *25*, 1416–1425.
14. Yoon, Y.; Park, S.J.; Kim, D.R.; Lee, K.S. Thermal performance improvement based on the partial heating position of a heat sink. *Int. J. Heat Mass Transf.* **2018**, *124*, 752–760.
15. Culham, J.R.; Khan, W.A.; Yovanovich, M.M.; Muzychka, Y.S. The influence of material properties and spreading resistance in the thermal design of plate fin heat sinks. *J. Electron. Packag.* **2007**, *129*, 76–81.
16. Ellison, G.N. Maximum thermal spreading resistance for rectangular sources and plates with nonunity aspect ratios. *IEEE Trans. Compon. Packag. Technol.* **2003**, *26*, 439–454.
17. Cho, E.S.; Choi, J.W.; Yoon, J.S.; Kim, M.S. Experimental study on microchannel heat sinks considering mass flow distribution with non-uniform heat flux conditions. *Int. J. Heat Mass Transf.* **2010**, *53*, 2159–2168.
18. Yoon, S.H.; Saneie, N.; Kim, Y.J. Two-phase flow maldistribution in minichannel heat-sinks under non-uniform heating. *Int. J. Heat Mass Transf.* **2014**, *78*, 527–537.
19. Lelea, D. The heat transfer and fluid flow of a partially heated microchannel heat sink. *Int. Commun. Heat Mass Transf.* **2009**, *36*, 794–798.
20. Toh, K.C.; Chen, X.Y.; Chai, J.C. Numerical computation of fluid flow and heat transfer in microchannels. *Int. J. Heat Mass Transf.* **2002**, *45*, 5133–5141.
21. Emekwuru, N.G.; Hall, F.R.; Spence, P.J. Partially heated heat sinks in a zero-bypass. *Int. Commun. Heat Mass Transf.* **2012**, *39*, 343–349.
22. Lee, M.; Kim, H.J.; Kim, D.K. Nusselt number correlation for natural convection from vertical cylinders with triangular fins. *Appl. Therm. Eng.* **2016**, *93*, 1238–1247.
23. Kim, D.K.; Han, I.Y.; Kim, S.J. Study on the steady-state characteristics of the sensor tube of a thermal mass flow meter. *Int. J. Heat Mass Transf.* **2007**, *50*, 1206–1211.
24. Liu, D.; Garimella, S.V. Analysis and optimization of the thermal performance of microchannel heat sinks. *Int. J. Numer. Methods Heat Fluid Flow* **2005**, *15*, 7–26.
25. Incropera, F.P.; Lavine, A.S.; Bergman, T.L.; DeWitt, D.P. *Fundamentals of Heat and Mass Transfer*, 6th ed.; John Wiley & Sons: Hoboken, NJ, USA, 2007; pp. 153–155.